BJR

RESEARCH

Evaluation of the histological and mechanical features of tendon healing in a rabbit model with the use of second-harmonic-generation imaging and tensile testing

E. Hase,
K. Sato,
D. Yonekura,
T. Minamikawa,
M. Takahashi,
T. Yasui

The Tokushima University, Tokushima, Japan

Objectives

This study aimed to evaluate the histological and mechanical features of tendon healing in a rabbit model with second-harmonic-generation (SHG) imaging and tensile testing.

Materials and Methods

A total of eight male Japanese white rabbits were used for this study. The flexor digitorum tendons in their right leg were sharply transected, and then were repaired by intratendinous stitching. At four weeks post-operatively, the rabbits were killed and the flexor digitorum tendons in both right and left legs were excised and used as specimens for tendon healing (n = 8) and control (n = 8), respectively. Each specimen was examined by SHG imaging, followed by tensile testing, and the results of the two testing modalities were assessed for correlation.

Results

While the SHG light intensity of the healing tendon samples was significantly lower than that of the uninjured tendon samples, 2D Fourier transform SHG images showed a clear difference in collagen fibre structure between the uninjured and the healing samples, and among the healing samples. The mean intensity of the SHG image showed a moderate correlation ($R^2 = 0.37$) with Young's modulus obtained from the tensile testing.

Conclusion

Our results indicate that SHG microscopy may be a potential indicator of tendon healing.

Cite this article: *Bone Joint Res* 2016;5:577–585.

Keywords: Tendon, Collagen, Healing, Second-harmonic-generation microscopy, Tensile testing

Article Focus

- To perform both Second-harmonic-generation (SHG) imaging and tensile testing in a rabbit model of tendon healing.
- To assess the correlation between the mean intensity of SHG images and Young's modulus.
- To evaluate the potential of SHG imaging to indicate histological and mechanical recovery in tendon healing.

Key messages

- The mean SHG intensity in the healing tendon significantly decreased to 17.9% of that of the control tendon, with a p-value of $p < 0.001$.
- There was a moderate correlation ($R^2 = 0.37$) between the mean SHG intensity and Young's modulus.

Strengths and limitations

- This is the first study to analyse both SHG imaging and tensile testing on the same sample in a rabbit model of tendon healing.
- The small sample size limits the precision of the results and further work is necessary to explore the role of SHG microscopy in tendon healing.

E. Hase, MSc, Research Associate, Graduate School of Advanced Technology and Science, The Tokushima University, Tokushima 770-8506, Japan.
K. Sato, PhD, Associate Professor,
D. Yonekura, PhD, Professor,
T. Minamikawa, PhD, Associate Professor,
T. Yasui, PhD, Professor, Graduate School of Science and Technology, The Tokushima University, Tokushima 770-8506, Japan.
M. Takahashi, MD, PhD, Surgeon, Department of Orthopaedic Surgery, Tokushima Prefectural Central Hospital, Tokushima, 770-8539, Japan.

Correspondence should be sent to T. Yasui, email; yasui.takeshi@tokushima-u.ac.jp

doi: 10.1302/2046-3758.511.BJR-2016-0162.R1

Bone Joint Res 2016;5:577–585.
Received: 29 June 2016;
Accepted: 6 October 2016

Introduction

The primary function of tendons is to transmit force generated by skeletal muscles to bones, thus facilitating locomotion.[1] To achieve this function, the primary constitution of tendons is mechanically-tough extracellular matrix (ECM). The ECM of tendons is comprised mainly of collagen, which accounts for approximately 60% to 85% of the dry weight of tendons.[2] Collagen has uniform higher-order structures of microfibrils, fibrils, fibres, and fascicles, all of which are uniaxially oriented along the direction of the long axis in tendons. Such characteristic collagen structures ensure that tendons have high mechanical strength.

Mechanical load, as well as age and inflammation, are risk factors for a partial or complete tendon rupture. The healing process of the ruptured tendon consists largely of the proliferation and differentiation of tenoblasts around the injured area, the production of collagen and other ECM components, and alteration of the non-orientated coarsely distributed structure of collagen fibres into a uniaxially-oriented, densely-distributed structure (maturation).[3] However, it is often difficult to regain the same level of mechanical strength as before injury, and disruption or re-rupture of the tendon during the healing process is not uncommon.[4]

The process of tendon healing has been experimentally studied through various modalities, such as histology and mechanical testing. The staining method is straightforward because it reveals the orientation, density, and arrangement of the high-order structure of collagen. Haematoxylin-Eosin (HE) staining[5] as well as other methods[6] have been shown to demonstrate the histological recovery of a ruptured tendon. On the other hand, tensile testing is a direct method of evaluating the mechanical healing of a ruptured tendon.[7] Unfortunately, both methods of evaluation are invasive and destructive, and cannot be clinically applied to normal tendon healing. Currently, there is no established evaluation system clinically applicable to tendon healing.

Second-harmonic-generation (SHG) microscopy[8] is a promising tool for *in situ* observation of collagen fibres in tissues. SHG microscopy is known to be a good imaging modality that allows identification of collagen molecules with high selectivity, good image contrast, high spatial resolution, optical 3D sectioning and moderate penetration. Recently, SHG microscopy has been applied to analyse fatigue, damage, and/or inflammation and its efficacy has been demonstrated.[9-12] Considering that the SHG light intensity depends on the structural maturity, density, and aggregates of collagen molecules, SHG microscopy may be a promising probe for visualising the level of tendon healing without histological sectioning and staining.

In the present study, we demonstrate SHG imaging followed by tensile testing on tendon specimens in a rabbit model of tendon healing. Based on this approach, we assessed a correlation between the mean SHG intensity and the Young's modulus of tendon samples in order to investigate the reliability of SHG imaging in the process of tendon healing in comparison with mechanical testing. The present study was designed as a preliminary investigation into the potential utility of SHG microscopy as a clinical probe to assess tendon healing.

Materials and Methods

Rabbit model of tendon healing. The experimental protocol used in this study was approved by the Bioethics Committee for Animal Experiments at The Tokushima University. A rabbit model of tendon healing was prepared following the method used in previous research by another group.[13] In total, eight male Japanese white rabbits (eight to ten weeks old, weight 2.0 kg to 2.5 kg) were obtained from Kitayama Labes Co., Ltd. (Ina, Japan) and were individually housed in a climate-controlled animal care facility for one week in order to be acclimatised to a new environment. The rabbits were locally anesthetised with 1% lidocaine hydrochloride after inducing anaesthesia with the inhalation of isoflurane (5% for induction, 2% for maintenance, each with an air flow rate of 2 litres/minute). Following anaesthesia, the right leg was disinfected and shaved. The flexor digitorum tendon in the right leg was sharply transected by a No. 11 scalpel. The disrupted tendon was then repaired by intratendinous stitching with a looped 5-0 nylon suture. Postoperatively, the rabbits were individually housed in a climate-controlled animal care facility. To highlight the definite difference of collagen structure between the healing tendon and the control tendon, we performed the comparison at a single time-point of tendon healing. At four weeks post-operatively, the rabbits were euthanised by administering an overdose of sodium pentobarbitone (0.15 mg/kg BW). The flexor digitorum tendon in the right leg was excised as the healing tendon sample (n = 8), whereas that in the left leg was excised as the control (n = 8). Samples were kept frozen at -15 °C until evaluation. After being thawed at room temperature, each specimen was examined by SHG imaging, followed by tensile testing.

SHG imaging. Figure 1 shows the experimental setup of the inverted SHG microscope. We used a mode-locked Cr:Forsterite laser (CrF-65P, Avesta Ltd., Moscow, Russia, centre wavelength 1250 nm, pulse duration 70 fs, repetition rate 73 MHz) to enhance the depth of penetration in SHG imaging.[14] The mean power of the laser output light was adjusted to 20 mW at the sample surface by using a combination of a half-wave plate (HWP; CWO-1250-02-10, Lattice Electro Optics Inc., California, retardation tolerance = $\lambda/500$) and a polariser (P; PGL8610, CASIX Inc., Fujian, China, extinction ratio < 1×10^{-6}). Its linear polarisation was converted into circular polarisation by a quarter-wave plate (QWP; CWO-1250-04-10,

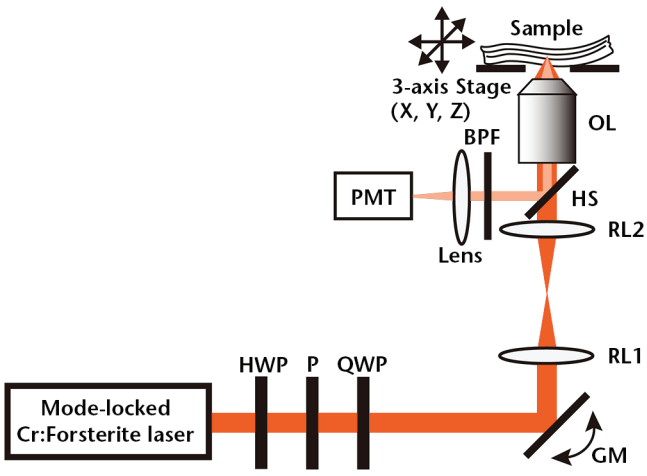

Fig. 1

Diagram showing the experimental setup of an inverted SHG microscope (HWP, half-wave plate; P, Polariser; QWP, quarter-wave plate; GM, galvanometer mirror; RL1 and RL2, relay lenses; HS, harmonic separator; OL, objective lens; BPF, optical band-bass filter; PMT, photon-counting photomultiplier).

Lattice Electro Optics Inc., retardation tolerance = λ/500) in order to cancel the polarisation dependence of the SHG efficiency of the orientated collagen fibres. The focal point of the laser beam was two-dimensionally scanned on a sample by a combination of a galvanometer mirror (GM), relay lenses (RL1 and RL2), and an objective lens (OL; CFI Plan 50 × H, Nikon Corp., Tokyo, Japan, magnification ×50, numerical aperture 0.9, working distance 350 μm, oil-immersion type). Backscattered SHG light was collected by the same OL, was reflected by a harmonic separator (HS; LWP-45-Runp625-Tunp1250-B-1013, Lattice Electro Optics Inc., Fullerton, California, reflected wavelength 625 nm), passed through an optical filter with a sharp pass-band (BPF; 625/26 nm BrightLine, Semrock Inc., Rochester, New York, pass wavelength 612 nm to 638 nm), and was then detected by a photon-counting photomultiplier with Peltier cooling (PMT; H7421-40, Hamamatsu Photonics K.K., Hamamatsu, Japan). Using the above GM optics, SHG images of a 400 μm × 400 μm region, composed of 256 pixels × 256 pixels, were acquired at a rate of 0.5 images/second. The range of probing depth in the present system was 0 ~ 200 μm from the sample surface, which was limited by the working distance (350 μm) of the OL and the thickness (120 ~ 170 μm) of a cover glass between the OL and the sample, and not limited by the penetration depth (~several hundred μm) of the 1250 nm laser light. To expand the lateral imaging region, we scanned the sample position at intervals of 400 μm using a stepping-motor-driven 3-axis translation stage every time an SHG image was obtained by the GM. Finally, we obtained a large-area SHG image with a size of 3.2 mm × 3.2 mm by stitching together 64 SHG images in a matrix of eight rows and eight columns. The total image acquisition time was around 15 minutes for one sample. During the experiment for SHG imaging, the sample was immersed in the physiological saline solution to avoid tissue dehydration. Although the sample temperature was not controlled, we consider the assessment to be unaffected. There was no load on the tendon when SHG imaging was performed. For calculation of the mean SHG light intensity, we used the large-area SHG images without contrast enhancement. In addition, image analysis based on 2D Fourier transform was performed using the magnified SHG images without or with contrast enhancement. The presence or absence of contrast enhancement did not influence results because we used the shape of the 2D Fourier transform spectrum.

Tensile testing. Tensile testing was undertaken immediately in order to avoid tissue degradation. We used a commercial tensile testing machine (EZ - S, Shimadzu Corp., Kyoto, Japan, load capacity 500 N, load cell precision ±1 %) for evaluating mechanical strength in the healing tendon. A single excised tendon fascicle was selected and the cross-section of the fascicle was estimated from the major and minor axes in the elliptically shaped cross-section of the fascicle. The tendon fascicle was then stretched at a tensile rate of 2 cm/min. Young's modulus was calculated from the stress–strain curve, in which we used the nominal stress and assumed that the cross-section did not change during the tensile test.

Statistical analysis. The data for mean SHG light intensity were reported as mean and standard deviation (SD). P-values < 0.001 and < 0.05 represented statistical significance and were used for statistical tests of mean SHG intensity and Young's modulus, respectively. Two group comparisons were made using Student's *t*-test. For the correlation between the mean SHG intensity and Young's modulus, the coefficient of determination (R^2) was used.

Results

SHG imaging. Since the SHG image indicated the highest intensity and the best contrast at a depth of 100 μm from the sample surface, we selected this depth for comparison of the collagen structure. First, we performed SHG imaging on the control samples. Figure 2a shows a comparison of the large-area SHG images without contrast enhancement (image size 3.2 mm × 3.2 mm, pixel size 2048 pixels × 2048 pixels) for three out of eight control samples (control (A), (B), and (C)) as representatives, although we performed the SHG imaging for all samples. The distribution of strong SHG light intensity was observed for all of them. Furthermore, thick collagen fibres were uniformly orientated parallel to the long axis of the tendon (vertical direction). When the region of the control (A) in Figure 2a (orange box) was magnified, as shown in Figure 2b (image size 400 μm × 400 μm, pixel size 256 pixels ×

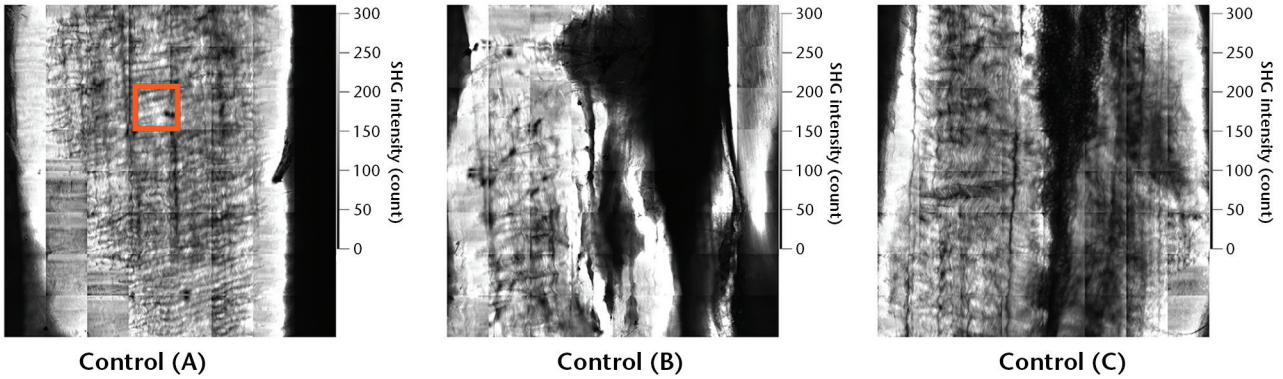

Fig. 2a

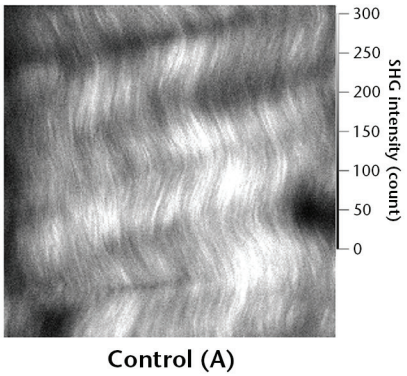

Fig. 2b

a) Comparison of the large-area second-harmonic-generation images without contrast enhancement (image size 3.2 mm × 3.2 mm, pixel size 2048 pixels by 2048 pixels) for three out of eight control samples (control (A), (B), and (C)); b) magnified image of the region of the control (orange box) (A) in (a). Image size is 400 µm × 400 µm, composed of 256 pixels × 256 pixels.

256 pixels), a crimp structure of thick collagen fibres was observed. Since these characteristics are consistent with the histological views of tendon tissue,[5,6] we can conclude that SHG imaging provides an accurate histological visualisation of collagen fibres in tendon without the need for histological sectioning and staining.

Next, we performed SHG imaging on the healing tendon samples. The disrupted portion had reconnected four weeks post-operatively. After eliminating scar tissue around the disrupted portion using a scalpel, we visualised a collagen structure of the healing tendon tissue at a depth of 100 µm from the sample surface. Figure 3 shows a comparison of the large-area SHG images without contrast enhancement (left column, image size 3.2 mm × 3.2 mm, pixel size 2048 pixels × 2048 pixels), the large-area SHG images with contrast enhancement (centre column, the same size as the left column), and the magnified SHG images with contrast enhancement (right column, image size 400 µm × 400 µm, pixel size 256 pixels × 256 pixels, corresponding to the region in the centre column orange box) among six out of eight healing samples (healing (A), (B), (C), (D), (E), and (F)) as representatives. From a comparison of SHG images without contrast enhancement between the control and the healing samples (Fig. 2a and the left column in Fig. 3), the SHG light intensity considerably decreased in all of the healing samples. The contrast-enhanced SHG images in the centre column and their magnified SHG images in the right column enabled visualisation of the fibrous structure of the collagen in the healing area more clearly. In contrast to the control sample, the healing samples did not show clear crimp structures of thick collagen fibres. In addition, we observed that the collagen fibres in the healing samples were thin, somewhat oriented, and/or unevenly distributed.

The regenerated tissue in healing tendon mainly contains type-1 and type-3 collagen, whereas native tissue in the control tendon mainly contains that of type-1 collagen only.[15] Although type-3 collagen has less higher-order fibre structure than type-1 collagen,[16] there is no significant difference in SHG light efficiency between type-1 and type-3 collagen.[17] We consider the SHG light intensity closely related with the degree of structural maturity, rather than the difference in type of collagen. The disorganised, less-oriented, thin collagen fibre structure in the healing tendon decreases the mechanical strength and SHG light intensity, whereas

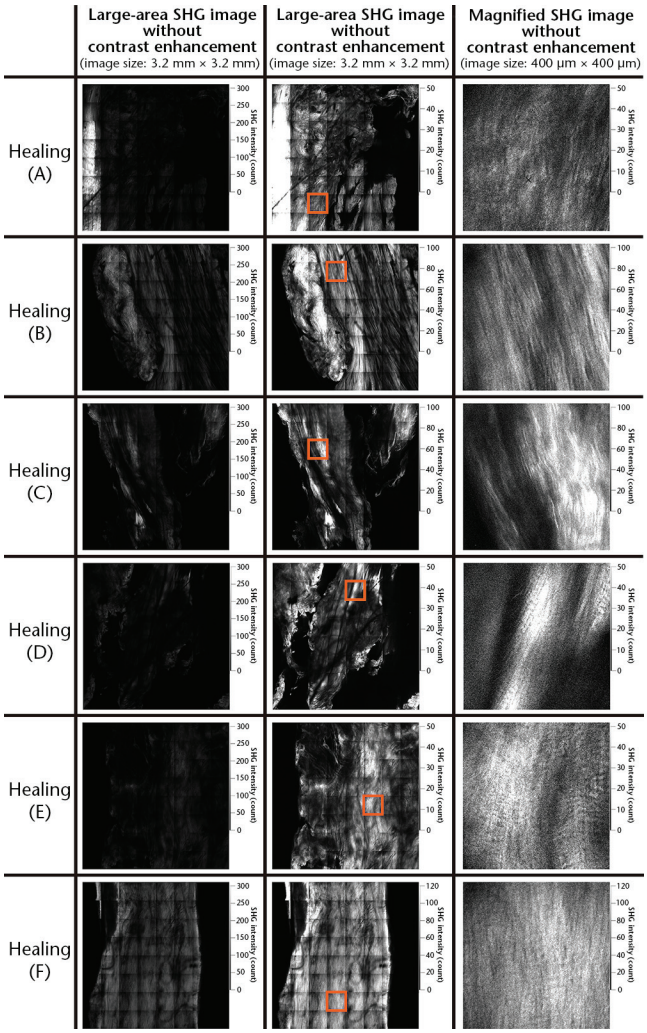

Fig. 3

Comparison of the large-area second-harmonic-generation (SHG) images without contrast enhancement (left column, image size 3.2 mm × 3.2 mm, pixel size 2048 pixels × 2048 pixels), the large-area SHG images with contrast enhancement (centre column, image size 3.2 mm × 3.2 mm, pixel size 2048 pixels × 2048 pixels), and the magnified SHG images with contrast enhancement (right column, image size 400 μm × 400 μm, pixel size 256 pixels × 256 pixels, corresponding to the region in the centre column; orange box) among six out of eight healing samples (healing (A), (B), (C), (D), (E), and (F)).

the well-organised, better-oriented, thick collagen fibre structure in the control tendon enhances mechanical strength and SHG light intensity.

We calculated the mean SHG light intensity of all pixels in the large-area SHG image without the contrast enhancement (see Fig. 2a and the left column in Fig. 3) for each sample to compare the SHG light intensity of the healing samples with that of the control samples quantitatively. Figure 4 shows a comparison of the mean SHG light intensity between the control samples (n = 8) and the healing samples (n = 8). The mean SHG light intensity was 201 (SD 37) counts for the control samples and 36 (SD 21) counts for the healing samples, respectively. The mean SHG light intensity in the healing samples was

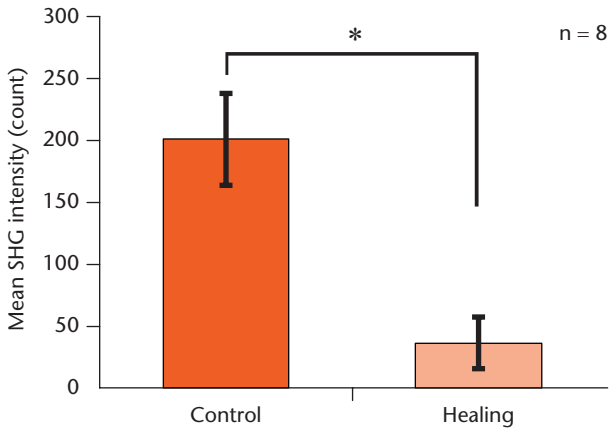

Fig. 4

Comparison of mean second-harmonic-generation intensity between the control (n = 8) and the healing samples (n = 8). Error bar shows the standard deviation of the data. *p < 0.001 (Student's *t*-test).

17.9% of that in the control samples. These differences were statistically significant (p < 0.001) and may indicate that the collagen fibres were still immature even though the repaired portion had apparently united (shown through gross visualisation).

Tensile testing. Immediately after the SHG imaging, tensile testing was performed on the same samples. Figure 5 shows the stress–strain curves for controls (A), (B), and (C) as representatives, although we performed the tensile testing for all samples. The curves of all the control samples presented similar profiles. The strain nonlinearly increased at low stress, and then linearly increased with the stress, indicating elastic deformation. The appearance of the peak after the linear region did not indicate the yield point but indicated slipping of the sample from the mechanical clamp. As a result, we did not include the other mechanical properties such as ultimate strength in this study.

Next, we performed tensile testing on the healing samples. Figure 6 shows the stress–strain curves for healing (A), (B), and (C), respectively. Unlike the curves of the control samples, the linear region of the healing samples was considerably less steep than that of the control samples.

Young's modulus was calculated by applying linear fitting to the linear region of the stress–strain curve, as shown by the orange lines in Figures 5 and 6. Figure 7 shows a comparison between the Young's modulus of the control samples (n = 8) and the healing samples (n = 8). Young's modulus was 0.63 MPa (SD 0.15) for the control samples and 0.36 MPa (SD 0.23) for the healing samples. Young's modulus in the healing samples was 57.1 % of that in the control samples, and this difference was statistically significant (p < 0.05). These results indicated that mechanical recovery of the healing samples was still imperfect at four weeks post-operatively.

Correlation between mean SHG light intensity and Young's modulus. As both the mean SHG light intensity and

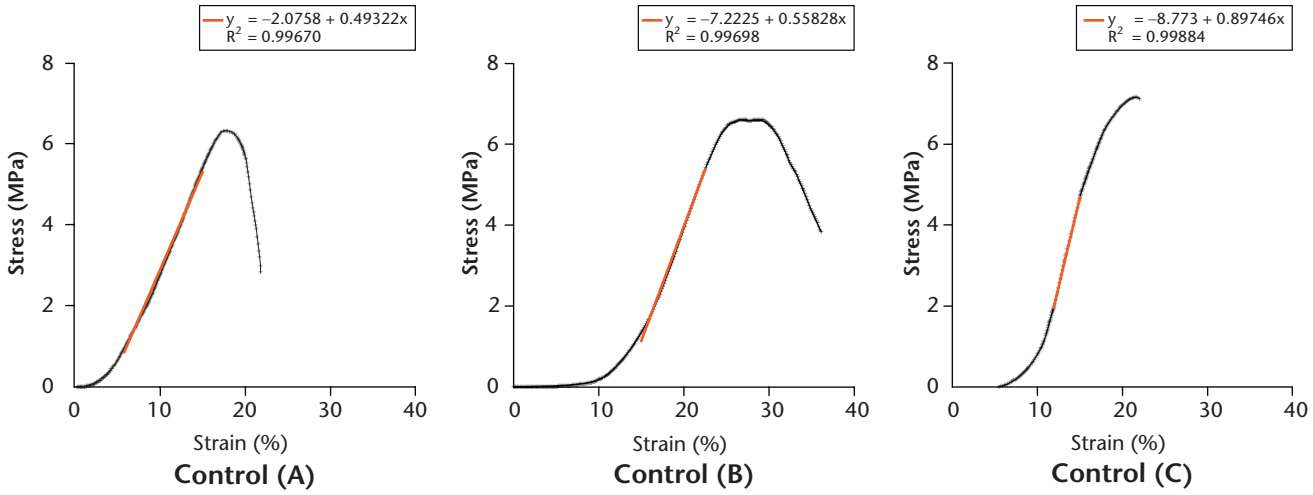

Fig. 5

Stress–strain curves of controls (A), (B), and (C). Orange lines show the result of the linear fitting to the linear increasing region in the stress-strain curve.

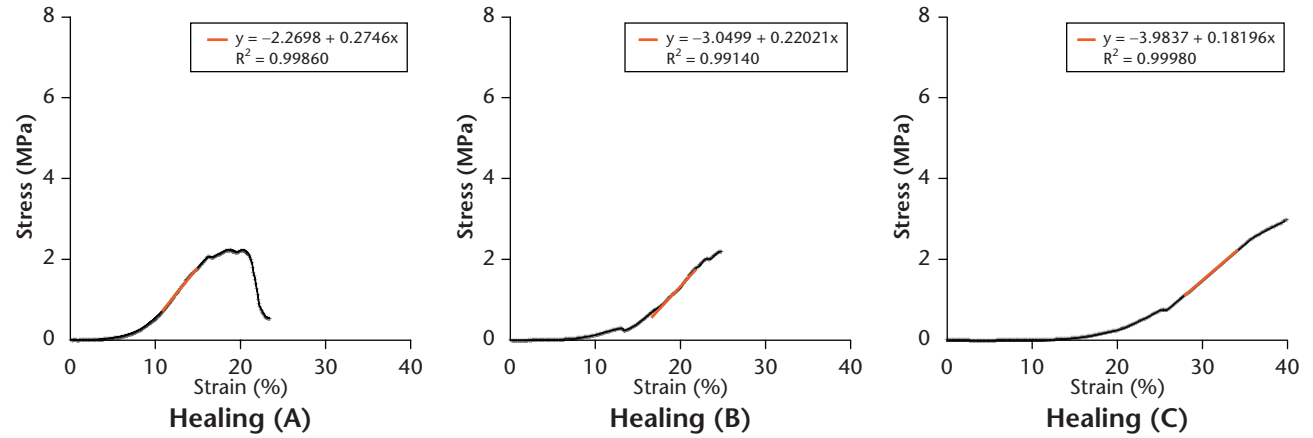

Fig. 6

Stress-strain curves of healing (A), (B), and (C). Orange lines show the result of the linear fitting to the linear increasing region in the stress-strain curve.

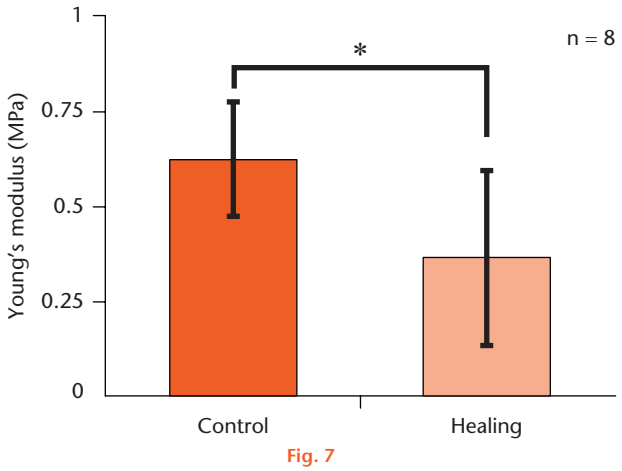

Fig. 7

Comparison of Young's modulus between the control samples (n = 8) and the healing samples (n = 8). Error bar shows the standard deviation of the data. *p < 0.05 (Student's *t*-test).

Young's modulus were obtained from the same sample, we calculated the correlation between the mean SHG light intensity and Young's modulus. Figure 8 shows the relation between the two sets of data, in which square and circle plots, respectively, indicate the data for eight control samples and eight healing samples. The control samples were distributed in the area of high SHG intensity and large Young's modulus, whereas the healing samples indicated low SHG intensity, with some variance in Young's modulus. From the data plots in Figure 8, we determined the coefficient of determination (R^2) to be 0.37 for both control and healing samples (see line in Figure 8).

Discussion

We performed SHG imaging of the healing tendon after removal of scar tissue. One may query whether such

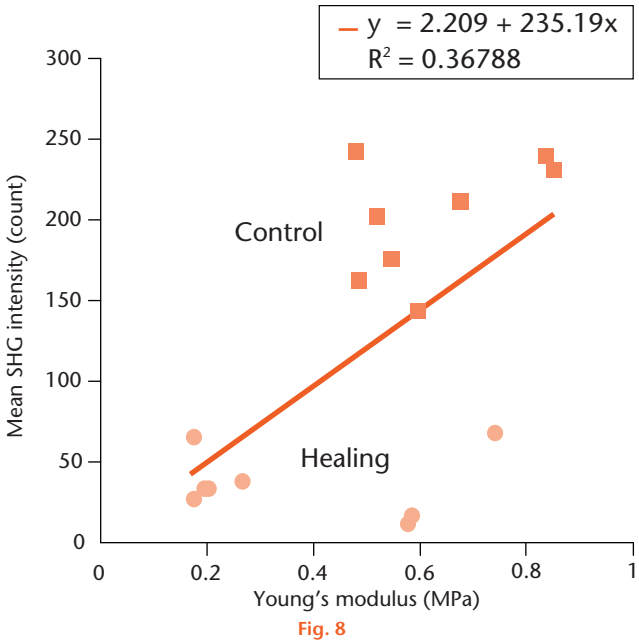

Fig. 8

Correlation between mean second-harmonic-generation light intensity and Young's modulus. Square plots show the control samples (n = 8), whereas circle plots show the healing sample (n = 8). Line shows the result of linear fitting to the plots of both control and healing samples, respectively.

approach can be used as a clinical probe for the evaluation of tendon healing, which is classified into intrinsic and extrinsic healing.[4] The formation of a scar is related to extrinsic healing. For example, if one were to remove scar tissue, it could hinder extrinsic healing because the scar tissue becomes mature and is embedded in the regenerated tissue. In this study, as the scar tissue was not completely unified with tendon tissue at four weeks post-operatively, we performed SHG imaging of the healing tendon after removal of the scar tissue in order to visualise collagen fibres in the tendon tissue itself. On the other hand, at the late stage of healing, it is difficult to discriminate the scar tissue from the tendon itself due to remodelling, and the scar tissue may give information on the degree of extrinsic healing. If we could quantitatively estimate overall healing by SHG imaging in the scar tissue of the repaired portion, it may be useful in order to evaluate tendon healing. Although we demonstrated *ex vivo* visualisation of the collagen fibres in tendon healing with SHG microscopy, the combination of SHG microscopy and a state-of-the-art fibre-optic probe with an outer diameter of 2 mm[18] may be used in the development of a clinical probe of tendon healing.

In the analysis of SHG images, we extracted the mean SHG intensity as the simplest parameter and evaluated the validity of this parameter for assessing tendon healing. However, when a quantitative analysis of SHG imaging is performed based on the SHG light intensity, one must consider the additional contributions other than the density and the structural maturity of the collagen fibres. This is because the SHG light intensity also depends on the incident light intensity, the optical property (surface reflection, absorption, or scattering) of the sample, and the probing depth of the objective lens. These factors may result in some error bars in Figure 4 and limit the R^2 value to 0.37 in Figure 8.

For a more precise analysis of SHG images, one would need to use other SHG parameters independent from SHG light intensity. One potential method is the image-based analysis with 2D Fourier transformation (2D-FT), which provides a 2D map of spatial frequency components in SHG images.[11,19] We show the preliminary results of this image analysis for the control and healing sample in order to demonstrate potential for tendon healing evaluation. Figure 9a shows the 2D-FT-SHG image of the control (A) in Figure 2b. The thick bowtie pattern is due to the uniform crimp structure of thick collagen fibres along the vertical direction. On the other hand, Figure 9b shows the 2D-FT-SHG images of three healing samples (healing (A), (B), and (C)) in the right column in Figure 3. The circular pattern in healing (A) is a result of disorganised collagen fibre structure without the specific orientation, implying immature healing. The thin bowtie pattern in the healing (B) is due to the collagen fibre structure with moderate orientation and less crimp structure, implying normal healing. The somewhat thick bowtie pattern in the healing (C) indicates the collagen fibre structure with moderate orientation and crimp structure, implying smooth healing. In this way, the 2D-FT-SHG image analysis has the potential to reflect the structural difference of collagen fibres with greater sensitivity, not only between the control sample and the healing sample, but also among the healing samples at different stages of healing.

The R^2 value between the mean SHG light intensity and Young's modulus was 0.37 (Fig. 8). It is possible that the sample size is too small for precise correlation evaluation. Another possible reason for the limited R^2 value may be the evaluation of tendon healing at only a single time point (four weeks post-operatively) although we performed the comparison at this time point to highlight the definite difference of collagen structure. Additional time points may clarify the validity of the mean SHG light intensity as an indicator of mechanical recovery of the repaired tendon.

In conclusion, we investigated histological and mechanical features of recovery in a rabbit model of tendon healing by using SHG imaging and tensile testing, respectively. This combination enabled us to evaluate collagen fibres histologically and to obtain Young's modulus on the single sample due to the *in situ* imaging capability of SHG microscopy without the need to perform staining. Because the collagen dynamics visualised by SHG microscopy are closely related to the

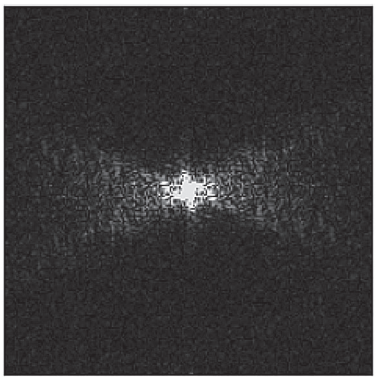

Control (A)

Fig. 9a

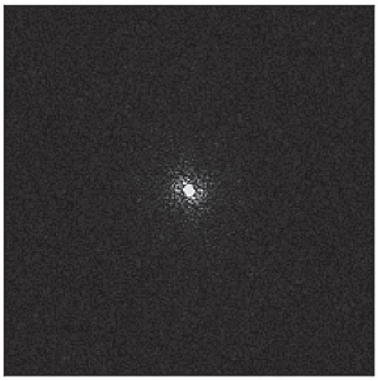

Healing (A)

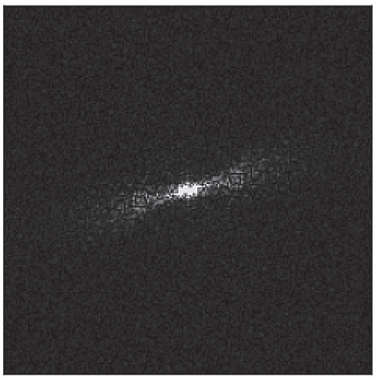

Healing (B)

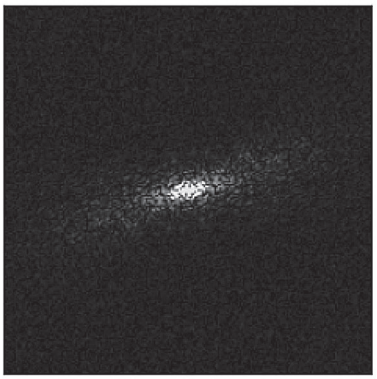

Healing (C)

Fig. 9b

a) 2D Fourier transformation second-harmonic-generation (2D-FT-SHG) image of the control (A) in Figure 2b (image size 400 μm^{-1} × 400 μm^{-1}, pixel size 256 pixels × 256 pixels). b) 2D-FT-SHG images of three healing samples (healing (A), (B), and (C)) in the right column of Figure 3 (image size 400 μm^{-1} × 400 μm^{-1}, pixel size 256 pixels × 256 pixels).

mechanical properties of the tendon, as well as its histology, a moderate correlation was confirmed between the mean SHG light intensity and Young's modulus. Furthermore, 2D-FT-SHG image analysis shows a potential for more precise analysis of tendon healing. If these approaches are investigated in a larger sample size, SHG microscopy may be more useful for evaluation of histological and mechanical features of recovery in healing tendons.

References

1. **Bojsen-Møller J, Magnusson SP, Rasmussen LR, Kjaer M, Aagaard P.** Muscle performance during maximal isometric and dynamic contractions is influenced by the stiffness of the tendinous structures. *J Appl Physiol (1985)* 2005;99:986-994.
2. **Kastelic J, Galeski A, Baer E.** The multicomposite structure of tendon. *Connect Tissue Res* 1978;6:11-23.
3. **Carlstedt CA, Madsen K, Wredmark T.** Biomechanical and biochemical studies of tendon healing after conservative and surgical treatment. *Arch Orthop Trauma Surg* 1986;105:211-215.
4. **Sharma P, Maffulli N.** Tendon injury and tendinopathy: healing and repair. *J Bone Joint Surg [Am]* 2005;87-A:187-202.
5. **Longo UG, Franceschi F, Ruzzini L, et al.** Characteristics at haematoxylin and eosin staining of ruptures of the long head of the biceps tendon. *Br J Sports Med* 2009;43:603-607.
6. **Cetti R, Junge J, Vyberg M.** Spontaneous rupture of the Achilles tendon is preceded by widespread and bilateral tendon damage and ipsilateral inflammation: a clinical and histopathologic study of 60 patients. *Acta Orthop Scand* 2003;74:78-84.
7. **Jung HJ, Fisher MB, Woo SLY.** Role of biomechanics in the understanding of normal, injured, and healing ligaments and tendons. *Sports Med Arthrosc Rehabil Ther Technol* 2009;1:9.
8. **Campagnola PJ, Dong CY.** Second harmonic generation microscopy: principles and applications to disease diagnosis. *Laser Photonics Rev* 2011;5:13-26.
9. **Sereysky JB, Andarawis-Puri N, Jepsen KJ, Flatow EL.** Structural and mechanical effects of *in vivo* fatigue damage induction on murine tendon. *J Orthop Res* 2012;30:965-972.
10. **Pingel J, Wienecke J, Kongsgaard M, et al.** Increased mast cell numbers in a calcaneal tendon overuse model. *Scand J Med Sci Sports* 2013;23:e353-e360.
11. **Fung DT, Sereysky JB, Basta-Pljakic J, et al.** Second harmonic generation imaging and Fourier transform spectral analysis reveal damage in fatigue-loaded tendons. *Ann Biomed Eng* 2010;38:1741-1751.
12. **Abraham T, Fong G, Scott A.** Second harmonic generation analysis of early Achilles tendinosis in response to *in vivo* mechanical loading. *BMC Musculoskelet Disord* 2011;12:26.
13. **Leppilahti J, Puranen J, Orava S.** Incidence of Achilles tendon rupture. *Acta Orthop Scand* 1996;67:277-279.
14. **Yasui T, Takahashi Y, Ito M, Fukushima S, Araki T.** *Ex vivo* and *in vivo* second-harmonic-generation imaging of dermal collagen fiber in skin: comparison of imaging characteristics between mode-locked Cr:forsterite and Ti:sapphire lasers. *Appl Opt* 2009;48:D88-D95.
15. **Lin TW, Cardenas L, Soslowsky LJ.** Biomechanics of tendon injury and repair. *J Biomech* 2004;37:865-877.

16. **Chang S-W, Shefelbine SJ, Buehler MJ.** Structural and mechanical differences between collagen homo- and heterotrimers: relevance for the molecular origin of brittle bone disease. *Biophys J* 2012;102:640-648.
17. **Cox G, Xu P, Sheppard C, Ramshaw J.** Characterization of the second harmonic signal from collagen. *Proc SPIE* 2003;4963:32-40.
18. **Zhang Y, Akins ML, Murari K, et al.** A compact fiber-optic SHG scanning endomicroscope and its application to visualize cervical remodeling during pregnancy. *Proc Natl Acad Sci U S A* 2012;109:12878-12883.
19. **Rao RAR, Mehta MR, Toussaint KC Jr.** Fourier transform-second-harmonic generation imaging of biological tissues. *Opt Express* 2009;17:14534-14542.

Funding Statement
- A Grant-in-Aid for Scientific Research 25560200 and 26246031 has been received for this study from the Japan Society for the Promotion of Science.

Author Contribution
- E. Hase: Built the instrument, Performed the experiment, Data analysis, Writing the paper.
- K. Sato: Contributed to manuscript preparation.
- D. Yonekura: Contributed to manuscript preparation.
- T. Minamikawa: Contributed to manuscript preparation, Data analysis.
- M. Takahashi: Conceived the idea and supervised the research.
- T. Yasui: Conceived the idea and supervised the research.

ICMJE COI Statement
- None declared